Influence of the heat transfer fluid in a CSP plant molten salts charging process

Gerard Peiró[1], Jaume Gasia[1], Laia Miró[1], Cristina Prieto[2], Luisa F. Cabeza[1,*]

[1]GREA Innovació Concurrent, INSPIRES Research Centre, Universitat de Lleida, Pere de Cabrera s/n, 25001, Lleida, Spain

[2]Abengoa Research. C/Energía Solar 1, 41012, Seville, Spain

*Corresponding author: Email: lcabeza@diei.udl.cat

Abstract

The selection of a proper heat transfer fluid (HTF) is a key factor to increase the efficiency of concentrated solar power plants and therefore, to reduce their internal associated CAPEX (capital expenditures of developing and constructing a plant, excluding any grid-connection charges) and OPEX (operating expenditures from the first year of a project's operation). This paper presents a comparative study of two commercial HTF which are widely used in different industries and CSP plants: thermal oil Therminol VP-1 and silicone fluid Syltherm 800. First, the authors theoretically studied the properties of both HTF based on the data given by the manufactures. Afterwards, the authors experimentally perform the comparison in a two-tank molten salt thermal energy storage pilot plant built at the University of Lleida (Spain). The study is focused on the plate heat exchanger of the facility during several charging processes with a counter flow arrangement. Results from both studies showed that, for the same working conditions, Therminol VP-1 is the best candidate for the above-mentioned purposes due to its higher heat transfer, lower thermal losses and lower power consumption associated to the HTF pump. However, it presents problems a low crystallization point, which should also be considered.

Keywords: Heat transfer fluid; Therminol VP-1; Syltherm 800; Molten salts; Concentrated solar power plant; Plate heat exchanger

Nomenclature

A	Heat exchange area, m^2
b	Mean channel spacing, m
C	Heat capacity, W/ºC
C_h	Constant of plate heat exchanger Nusselt correllation
cp	Specific heat, J/kg·ºC
D	Diameter, m
E	Energy released/absorbed, kWh
G	Mass channel velocity, kg/m^2·s
h	Heat transfer coefficient or film coefficient, W/m^2·K
k	Thermal conductivity, W/m·K
L_c	Packed length, m
L_p	Vertical distance between ports, m
L_w	Effective channel width, m
$\dot{m}$	Mass flow rate, kg/s
N_{cp}	Number of channels per pass
N_p	Number of passes
N_t	Number of plates
Nu	Nusselt non-dimensional number, -
p	Plate pitch
Pr	Prandtl non-dimensional number, -
Q	Heat transfer rate, W
R	Function dependent of the measured variables
Re	Reynolds non-dimensional number, -
t	Plate thickness, m
T	Temperature, ºC
U	Overall heat transfer coefficient, W/m^2·K
W	Uncertainty in the final result
w	Uncertainty of independent variables
x	Independent measured variable

Greek symbols

ΔT	Temperature difference, ºC
β	Chevron angle, º
ε	Effectiveness, -
ϕ	Surface enlargement factor, -

μ	Viscosity, $N/s \cdot m^2$
η	Efficiency, -

Subscripts

b	Bulk heat exchanger
cor	Correlation
e	Equivalent
eff	Effective
Exp	Experimental
HTF	Heat transfer fluid
in	Inlet
LMTD	Log-mean temperature difference
max	maximum
min	minimum
n	Independent variables
out	Outlet
p	Projected
PHEX	Plate heat exchanger
salts	salts
s	Surface

1 Introduction

Concentrated solar power (CSP) plants have become one of the most developed and studied technologies worldwide. However, there is a lack of continuity on the generation of electricity due to their sunlight availability strong dependence. The incorporation of thermal energy storage (TES) technologies in the CSP plants allows solving this drawback, and therefore enables increasing the CSP plants capacity factor and their dispatchability. Gil et al. [1] reviewed the high temperature TES concepts in CSP plants. They classified the storage concepts into active (mainly two-tank and thermocline) and passive (mainly concrete and castable ceramics) and described the main characteristics of each one of them. Medrano et al. [2] reviewed the CSP plants worldwide which used TES systems and classified them according to Gil et al. [1]. An update review was later done by Liu et al. [3]. They showed that parabolic through is nowadays the most extended CSP technology, being present in the 80 % of the CSP plants in operation and under construction. Moreover, indirect two-tank molten salt TES system is the most installed TES technology in this type of CSP plants. This consists of two storage tanks (usually referred as cold and hot) filled with molten salt where the energy is stored in sensible form. The molten salt from the cold storage tank (298 ºC) are heated up in a heat exchanger by a heat transfer fluid (HTF), generally thermal oil, coming from the parabolic trough solar field (391 ºC). Then, the heated molten salts are stored in the hot storage tank (385 ºC). When the stored energy is needed, the system operates in reverse form to heat up the HTF (Figure 1).

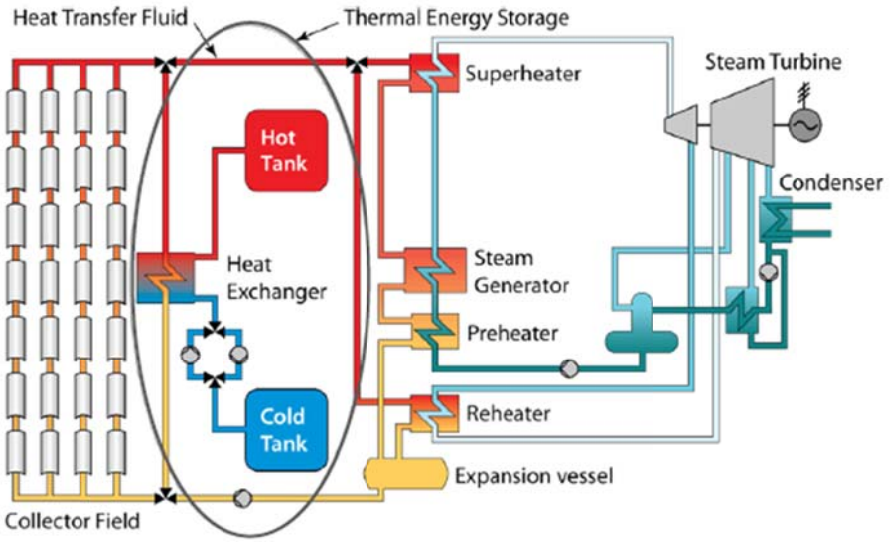

Figure 1. Scheme of parabolic trough power plant with an integrated two-tank molten salts TES system [4]

The two-tank molten salts system has been theoretically studied by describing the lessons learnt during the design, start-up and operation in low-scale experimental facilities (capacities ranging

between 0.3 MWh and 8 MWh) [5-7]. These studies showed the importance and helpfulness of developing pilot plant facilities within a scale range between the laboratory and real plants to achieve higher economy savings in real CSP plants. Hermann et al. [8] studied the technical and economic feasibility of a two-tank molten salt TES system linked to a parabolic trough CSP plant. They concluded that a storage system of 12 h at full load capacity reduced around 10 % the levelized electricity cost. Prieto et al. [9] experimentally evaluated the molten salts temperature distribution and the heat losses in the pilot plant facility presented in Cabeza et al. [6]. The results showed on one hand no temperature stratification in the storage tank, and on the other hand that the radial temperature distribution was mainly due to the insulation, the type of electrical resistance used for the molten salts temperature control, the orientation of the storage tanks, and the boundary conditions.

Glatzmayer [4] presents some guidelines to increase ~~of~~the efficiency of the system and therefore to make CSP electricity production more cost-effective. ~~He~~The author states that the TES system efficiency may be improved by developing new HTF, new components, and new operational strategies. The HTF thermally connects the solar field, the storage system, and the power block. Regarding to this topic, Benoit et al. [10] reviewed the existing and potential HTF used in the CSP -receivers and determined the main requirements for a proper HTF. First, the HTF should be able to work in an extended working temperature range and with a high thermal stability to increase the temperature and therefore increasing the efficiency of the cycle. Hence, the cost of the solar field, which turns to be the main saving factor in a CSP plant, can be reduced. Second, the HTF should have good thermophysical properties to increase the heat transfer between the TES material and the power block driving fluid, and to bear the high pressure and temperature changes. And third, the HTF should be non-hazardous, should have a good chemical behaviour in terms of corrosion and compatibility with the piping material and ~~HTF~~should be cost-effective. Similar to Benoit et al. [10], Vignarooban et al. [11], and Gasia et al. [12] reviewed the different types of HTF which are suitable for CSP plants and high temperature applications (liquids, supercritical fluids, and gases), their thermal and physical properties, their cost, and the most typical piping and container materials for HTF. They showed that thermodynamic cycle efficiencies could achieve values in a range between 35% and 42% by using thermal oil, molten salts or water/steam as HTF. They also showed that new HTF, which need to be stable at 700 ºC, are required to achieve thermodynamic cycle efficiencies of 50%. They proposed new molten salts, liquid metals, supercritical water, and carbon dioxide or pressurized gases and particles. Sau et al. [13] experimentally studied the behaviour of two different medium size plants (50 MWe), which used two different HTF: a binary mixture of $NaNO_3/KNO_3$ (64/36 mol%) and a ternary mixture of $NaNO_3/KNO_3/LiNO_3$ (37/45/18 mol%). Moreover, they performed an economic analysis to compare it with the thermal performance

results. Results showed that in terms of operation, the lower melting temperature of the ternary mixture is desired, while in terms of economics, both mixtures have practically the same final cost per kWh.

The efficiency of an indirect two-tank TES system may be improved by using a proper HTF. However, the fact of understanding the heat transfer process in the HTF-molten salt heat exchanger is also crucial in order to develop new operational strategies and therefore, to increase the performance of CPS plants. Nowadays, shell-and-tube heat exchangers are the most economic designs for CSP plants coupled with the two-tank molten salt TES system, but plate heat exchangers (PHEX) start to arise as candidates because they provide higher efficiencies and more flexibility than shell-and-tube heat exchangers despite the fact that they have lower mechanical resistance. The first study demonstrating the feasibility of a PHEX under real CSP plants working conditions was performed by Peiró et al [14], who analysed charging and discharging processes using molten salts and a commercial HTF. However, no experimental studies have been found in the literature focusing on the analysis of the influence of the HTF on the heat transfer in a PHEX for CSP plants. Hence, the objective of the present paper is to address this gap by studying two different commercial HTF widely used in the industry and CSP plant: the thermal oil Therminol VP-1 and the silicone fluid Syltherm 800. First, a theoretical study of both HTF is done by describing the impact of each thermophysical property in the different operational parameters of CSP plants. Second, an experimental study is performed by comparing the thermal performance of both HTF in a PHEX under different charging processes. To carry out the experimental study, the authors used the two-tank molten salt pilot plant constructed at the Universitat de Lleida [6].

2 Materials

2.1. Heat transfer fluids

Two HTF were considered for carrying out the experimentation: Therminol VP-1 [15] and Syltherm 800 [16]. Therminol VP-1 is a synthetic heat transfer oil which consists of a eutectic mixture of 73.5% diphenyl oxide ($C_{12}H_{10}O$) and 26.5% biphenyl ($C_{12}H_{10}$) while Syltherm 800 is a silicone fluid which is based on dimethyl polysiloxane $(C_2H_6OSi)n$. Figure 2 shows the molecular structure of the different organic compounds which are present in Therminol VP1 and Syltherm 800.

Regarding the health hazard, Therminol VP-1 is classified as a harmful by inhalation product, dangerous for the environment, especially for the aquatic environment. For this reason,

Therminol VP-1 must be manipulated with respiratory, skin and eyes protection under ventilated environments. The contact with oxidant agents must be avoided. Moreover, Therminol VP-1 waste must be recycled or burned according to the regulatory statements. On the other hand,Syltherm 800 presents a lower toxicity by inhalation and by contact with skin or eyes. Is practically non-toxic to aquatic and air organisms. For its manipulation, good general ventilation should be sufficient for most conditions. No respiratory protection should be needed. However, if material is heated or sprayed, the use an approved air-purifying respirator is recommended. Protection glasses and clothes are recommended. The generated waste of Syltherm 800 must be treated by incineration or other appropriated thermal destruction according to regulations.

Finally, regarding to economic aspects, Therminol VP-1 is cheaper than Syltherm 800, 3.07 €/kg and 41.64 €/kg, respectively.

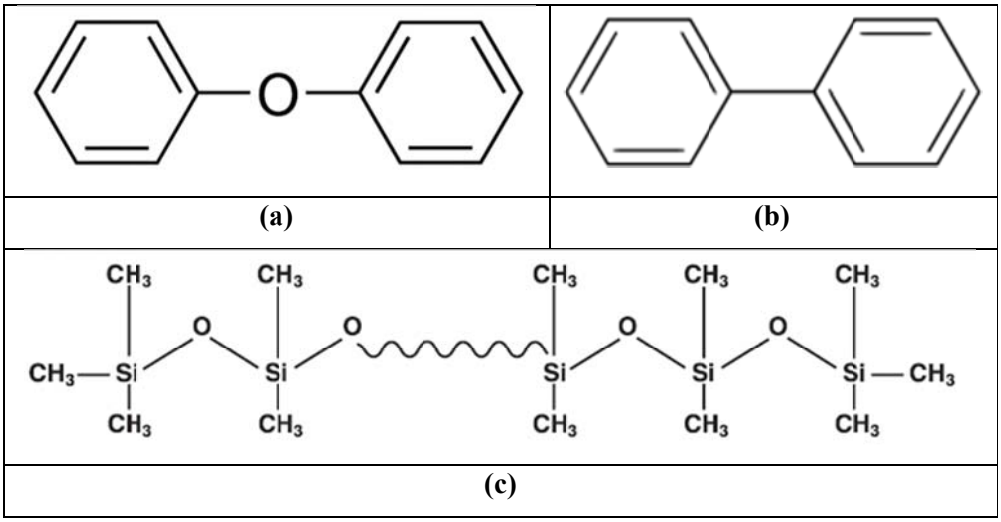

Figure 2. Molecular structure of (a) diphenyl oxide[17], (b) biphenyl [18], and (c) dimethyl polysiloxane [16]

2.2. TES material

The selected TES material was the binary eutectic mixture of 60 wt.% of sodium nitrate ($NaNO_3$) and 40 wt.% of potassium nitrate (KNO_3), also known as *molten salt* or *solar salt*. This material is widely used for TES purposes, mainly in CSP plants, and its thermophysical properties have been extensively studied and reviewed in previous research studies [19-22]. Moreover, the authors of the present study analysed and characterised the most important properties of molten salts, which are summarized in Table 1.

Table 1. Thermophysical properties of molten salts [Dr. Cristina Prieto, Abengoa, personal communication, April 27th, 2016]

Properties	**Values**
Composition	$NaNO_3$/ KNO_3 (60/40 wt.%)
Appearance	White crystalline in solid and clear yellow in liquid
Melting point	238-241 ºC
Density	$\rho(kg/m^3) = 0.636 \cdot T(^oC) + 2089.905$
Specific heat	$cp(kJ/kg \cdot K) = 1.723 \cdot 10^{-4} \cdot T(^oC) + 1.443$
Thermal conductivity	$\lambda(W/m \cdot K) = 1.9 \cdot 10^{-4} \cdot T(^oC) + 0.443$
Kinematic viscosity	$\upsilon(m^2/s) = -6.557 \cdot 10^{-14} \cdot T^3(^oC) + 1.055 \cdot 10^{-10} \cdot T^2(^oC) - 5.706 \cdot 10^{-8} \cdot T(^oC) + 1.112 \cdot 10^{-5}$

3. Experimental setup

The experimental studies presented in this work were carried out at the high temperature pilot plant facility located at the University of Lleida (Spain). It is composed of four main parts: the heating system, the cooling system, the storage system, and the heat exchange system (Figure 3). The heating system consists of a 24 kWe electrical heater. The cooling system consists of a 20 kWth air-HTF heat exchanger. The storage system consists of two molten salts storage tanks of 0.57 m^3 with the same aspect ratio than the storage tanks of real CSP plants. They contain 1000 kg of molten salts, which are stored and recirculated through the molten salts loop during the charging and discharging processes. Finally, the heat exchange system consists of an ALFANOVA HP 76-38H PHEX [23]. Figure 4a shows an overview of the PHEX installed in the experimental facility. Moreover Figure 4b and Table 2 show its main geometric and design characteristics. A more detailed description of the experimental facility can be found in Cabeza et al. [6].

With the aim of analysing the behaviour of the molten salts and the HTF during the charging process, all sensors used in the experimentation were connected to a data acquisition system and recorded at a time interval of 30 s to further be processed. The temperature of the molten salts and HTF at the inlet and outlet of the PHEX were measured with four Pt-100 resistance temperature detectors, which were located in well insulated tube sections at 83 mm from the four terminals of the PHEX. The HTF volumetric flow rate of was measured using a calibrated orifice plate with a differential pressure transmitter. Finally, the molten salts volume flow rate was calculated with a homemade device, which consists of a metallic tube that measures the molten salts level variation inside the hot tank during intervals of 5 minutes.

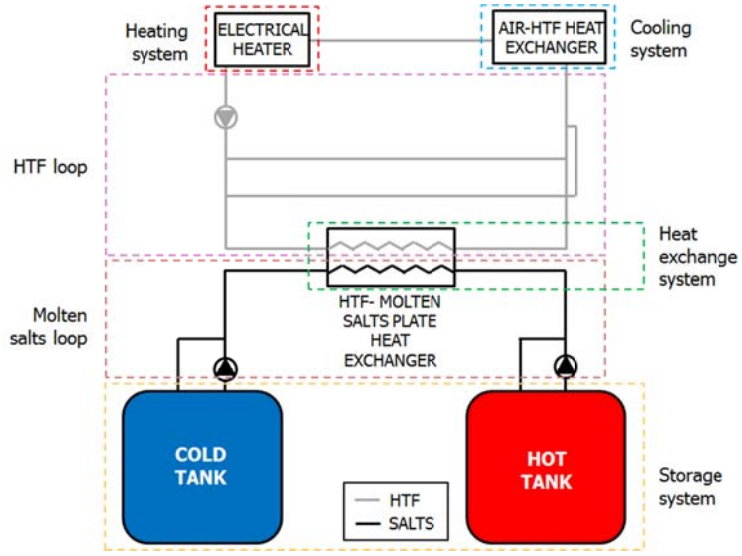

Figure 3. Schematic diagram of the high temperature pilot plant facility used to perform the experimentation

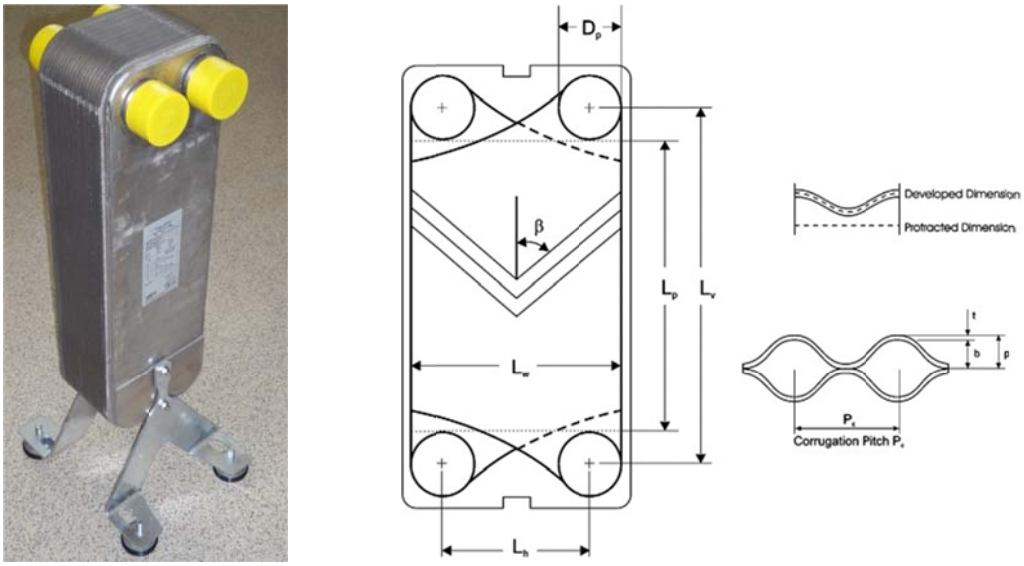

(a) **(b)**

Figure 4. Overview of the PHEX: (a) ALFANOVA HP 76-38H PHEX and (b) Schematic diagram [24]

Table 2. Design characteristics and technical properties of the ALFANOVA HP 76-38H PHEX used in the present experimentation

Characteristics	Thermal Oil side	Molten Salts side	Characteristics	
Design pressure	20 bar	10 bar	Number of plates, N_t	38
Design temperature	400 ºC	400 ºC	Effective channel width, L_w	191 mm
Directions of the fluids	Both	Both	Horizontal distance between centres of ports, L_h	92 mm
Length x Width x Height	208 x 191 x 618 mm		Vertical distance between centres of ports, L_v	519 mm
Plate material	Stainless steel alloy 316L		Vertical distance between ports, L_p	473 mm
Plate thickness, t	0.40 mm		Compressed plate pack length, L_c	208 mm
Number of passes, N_p	10 (both sides)		Port diameter, D_p	46 mm
Heat transfer area, A_{PHEX}	3.8 m^2		Corrugation pitch, P_c	n.a.
			Chevron angle, β	< 30 º

n.a. – not available

4. Methodology

4.1.Experimental procedure

The experimentation presented in this study consisted of several charging processes with two different HTF. However, before starting the charging process, a warming process was required to homogenize both the molten salts and the HTF at the initial temperature of charge, which were 293 ºC and 341 ºC, respectively. Once the homogenisation was achieved, the charging process started with an HTF mass flow rate of 0.08 kg/s, and a molten salts mass flow rate of 0.12 kg/s.-During this process, the molten salts were pumped from the cold storage tank to the hot storage tank passing through the PHEX in a counter-flow arrangement (Figure 5). The charging process was considered to be finished when the level of the molten salts in the cold tank reached 23-25 cm from the bottom of the tank, which is considered the minimum operation level of the pump.

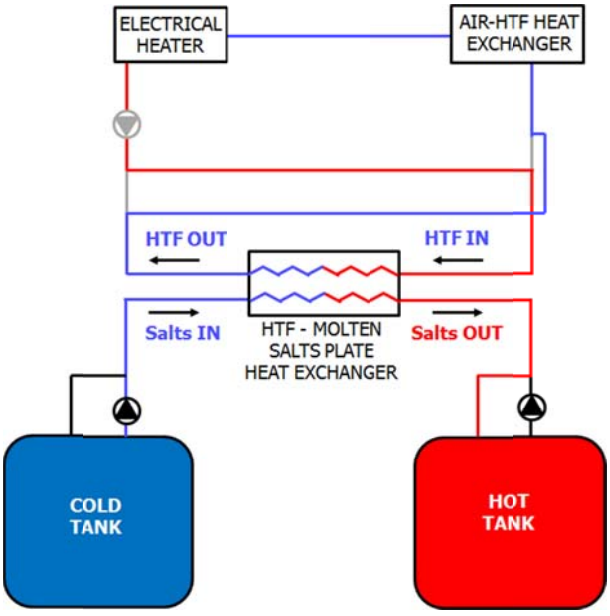

Figure 5. Flow diagram of the setup during a charging process in counter flow arrangement [14]

4.2. Analysis

The parameters used to compare the influence of the two evaluated HTF to the heat transfer at the PHEX are the temperature profiles, the overall heat transfer coefficient, the HTF convective heat transfer coefficients, the effectiveness, and the thermal efficiency, similarly to the work done by Tiwari et al. [25,26]. In this section the methodology for the calculation of the overall heat transfer coefficient (U), the thermal efficiency, and the effectiveness of the PHEX is presented.

In order to validate the U-values, two methodologies of calculation are presented. On one hand, the methodology from the energy balance at the PHEX. On the other hand, the methodology from the correlations of the convective heat transfer coefficients [24]. These methodologies were used under the following assumptions:

i. Steady-state fluid flow conditions for the PHEX operation.
ii. No heat is generated in the PHEX.
iii. The fluids properties are evaluated at film temperature of the fluid, with the exception of viscosity, which is also evaluated at the surface temperature.
iv. Uniform flow distribution through the PHEX.
v. Gravity forces are neglected.

4.2.1. Overall heat transfer coefficient (U) from the energy balance

The nominal heat transfer rate in the PHEX (Q_{PHEX}) is defined as the average heat transfer between the heat transfer at both the molten salts and the HTF sides of the PHEX (Eq. 1). Theoretically, both heat transfer rates should present the same values, but small differences due to heat losses and numerical errors in the measurements were experimentally observed [14].

$$Q_{PHEX} = \frac{Q_{salts} + Q_{HTF}}{2} \quad \text{Eq. 1}$$

The heat transfer absorbed by the molten salts (Q_{salts}) and heat released by HTF (Q_{HTF}) are derived from the following thermal balances (Eq. 2 and Eq. 3):

$$Q_{salts} = \dot{m}_{salts} \cdot cp_{salts} \cdot (T_{salts_{out}} - T_{salts_{in}}) \quad \text{Eq. 2}$$

$$Q_{HTF} = \dot{m}_{HTF} \cdot cp_{HTF} \cdot (T_{HTF_{in}} - T_{HTF_{out}}) \quad \text{Eq. 3}$$

Finally, the PHEX overall heat transfer coefficient from the energy balance (U_{Exp}) is derived from Eq. 4:

$$U_{Exp} = \frac{Q_{PHEX}}{A_{PHEX} \cdot \Delta T_{LMTD}} \quad \text{Eq. 4}$$

4.2.2. Overall heat transfer coefficient (U) from the convective heat transfer coefficients

The convective heat transfer coefficients at both the HTF and the molten salts sides of the PHEX are obtained from Eq. 5.

$$h = \frac{Nu \cdot k}{D_e} \quad \text{Eq. 5}$$

The Nusselt numbers for both fluids are obtained from Eq. 6 and Table 3. The Reynolds numbers (Eq. 7) is based on the mass channel velocity G (Eq. 8) and the equivalent diameter D_e (Eq. 9) of one plate channel of the PHEX:

$$Nu = C_h \cdot Re^n \cdot Pr^{1/3} \cdot \left(\frac{\mu_b}{\mu_s}\right)^{0.17} \quad \text{Eq. 6}$$

$$Re = \frac{D_e \cdot G}{\mu_b} \quad \text{Eq. 7}$$

$$G = \frac{\dot{m}}{N_{cp} \cdot b \cdot L_w} \quad \text{Eq. 8}$$

$$D_e = \frac{2b}{\phi} \quad \text{Eq. 9}$$

Table 3. Constants for a single-phase heat transfer calculation in chevron-PHEX [24]

Chevron angle (β)	Reynolds Number (Re)	C_h	n
≤ 30 º	≤ 10	0.718	0.349
	> 10	0.348	0.663

The number of channels per pass of the PHEX N_{cp} is defined by Eq. 10, the main spacing channel b is defined by Eq. 11, and the parameter surface enlargement factor ϕ is defined by Eq. 12:

$$N_{cp} = \frac{N_t - 1}{2N_p} \quad \text{Eq. 10}$$

$$b = p - t \quad \text{Eq. 11}$$

$$\phi = \frac{A_{eff}}{A_p} \quad \text{Eq. 12}$$

where p is the plate pitch in (Eq. 13), A_{eff} is the effective area of one plate (Eq. 14), and A_p is projected area of one plate (Eq. 15):

$$p = \frac{L_c}{N_t} \quad \text{Eq. 13}$$

$$A_{eff} = \frac{A_{PHEX}}{N_t} \quad \text{Eq. 14}$$

$$A_P = L_p \cdot L_w \quad \text{Eq. 15}$$

Finally, the PHEX overall heat transfer coefficient from the convective heat transfer coefficients (U_{cor}) is derived from Eq. 16:

$$U_{cor} = \frac{1}{\frac{1}{h_{HTF}} + \frac{t}{k_{PHEX}} + \frac{1}{h_{salts}}} \quad \text{Eq. 16}$$

4.2.3. Efficiency and effectiveness of the heat exchange

The efficiency of the heat exchange during the charging process is described as Eq. 17 shows, while its effectiveness is defined by Eq. 18:

$$\eta_{charge} = \frac{Q_{salts}}{Q_{HTF}} \quad \text{Eq. 17}$$

$$\varepsilon_{charge} = \frac{Q_{PHEX}}{Q_{max}} \quad \text{Eq. 18}$$

where Q_{max} is the maximum possible heat exchange rate with a given inlet temperatures and it is defined by Eq. 19:

$$Q_{max} = C_{min} \cdot (T_{HTF_{in}} - T_{salts_{in}}) \quad \text{Eq. 19}$$

where C_{min} is the lowest value from heat capacities of the HTF and the molten salts.

4.2.4. Uncertainty analysis

This section aims to show the uncertainties of the different parameters and their impact in the results of the present study to determine their precision and general validity. As above-explained, the evaluation of this study has been carried out at the PHEX. Therefore, the first step was to establish the uncertainties of the parameters which were measured during the experimentation and the uncertainties associated to the thermophysical properties of both the HTF and molten salts. These uncertainties were obtained from the technical data sheets of the sensors used for their measurement and from the available literature, and their values are shown in Table 4.

Table 4. Uncertainties of the different parameters involved in the analyses of the present study

Parameter	Units	Sensor	Uncertainty [± %]
HTF inlet temperature	[ºC]	Pt-100 1/5 Class B DIN	0.12
HTF outlet temperature	[ºC]	Pt-100 1/5 Class B DIN	0.12
Molten salts inlet temperature	[ºC]	Pt-100 1/5 Class B DIN	0.12
Molten salts outlet temperature	[ºC]	Pt-100 1/5 Class B DIN	0.12
HTF volume flow rate	[l/h]	Orifice plate	1.1
Molten salts level	[m]	Homemade device	1
HTF density	[kg/m^3]	[10]	3
HTF specific heat	[kJ/kg ºC]	[10]	3
HTF dynamic viscosity	[Pa·s]	[10]	3
HTF thermal conductivity	[W/m·ºC]	[10]	3
Molten salts density	[kg/m^3]	[27]	0.5
Molten salts specific heat	[kJ/kg ºC]	[27]	2.36
Molten salts dynamic viscosity	[Pa·s]	[27]	2.33
Molten salts Thermal conductivity	[W/m·ºC]	[27]	4.36

Once the uncertainties of these parameters were known, the next step was the estimation of the uncertainties of the calculated results, which were obtained as shown in Eq. 20 [28]:

$$W_R = \left[\left(\frac{\partial R}{\partial x_1}\cdot w_{x_1}\right)^2 + \left(\frac{\partial R}{\partial x_2}\cdot w_{x_2}\right)^2 + \cdots + \left(\frac{\partial R}{\partial x_n}\cdot w_{x_n}\right)^2\right]^{1/2} \quad \text{Eq. 20}$$

where W_R is the estimated uncertainty in the final result, R is a function which depends on the measured parameters, x_n are the independent measured parameters, and w_n are the uncertainties which are associated to the independent parameters.

Table 5 shows the estimated uncertainties of the different parameters evaluated in the present study. Notice that the calculated uncertainties for all the parameters which are presented in this study are lower than 10%.

Table 5. Estimated uncertainties of the parameters presented in the present study

Variable	HTF	Equation	Estimated uncertainty [± %]
Q_{HTF}	Therminol VP-1	Eq. 3	3.34
	Syltherm 800		3.33
Q_{salts}	Therminol VP-1	Eq. 3	2.65
	Syltherm 800		2.64
Q_{PHEX}	Therminol VP-1	Eq. 1	2.14
	Syltherm 800		2.20
h_{HTF}	Therminol VP-1	Eq. 5	8.01
	Syltherm 800		8.28
h_{salts}	Therminol VP-1		9.07
	Syltherm 800		8.55
U_{cor}	Therminol VP-1	Eq. 16	5.92
	Syltherm 800		6.25
U_{exp}	Therminol VP-1	Eq. 4	4.38
	Syltherm 800		7.66
ε_{charge}	Therminol VP-1	Eq. 18	5.06
	Syltherm 800		4.78
η_{charge}	Therminol VP-1	Eq. 17	5.79
	Syltherm 800		6.27

5. Results and discussion

5.1. Comparison of the thermophysical properties of both HTF

The thermophysical properties of the two HTF studied in this work are compared in this section. Moreover, the impact of each property in the operation of a CSP plant is analysed. Table 6 presents the empirical equations, based on the data given by the manufacturers, which are graphically represented in Figure 6 for a better comparison. It is observed that both HTF have thermal stabilities up to 400 ºC, which means that they are suitable for being used in parabolic through CSP plants. Regarding to the crystallization point, different values can be observed: while Syltherm 800 solidifies at -40 ºC, Therminol VP-1 does it at 12 ºC. Hence, the facilities where Therminol VP-1 is used should consider installing a tracing system in the piping system to avoid solidification problems in cold environments, and as a consequence, the OPEX would be higher. With reference to the density, Therminol VP-1 has higher values than Syltherm 800, which means that higher heat transfer rates can be obtained because the HTF is able to transport more mass per unit of volume. On the other hand, an HTF with higher density means that the fluid is heavier and therefore more pumping power is required. Hence, both the power required by HTF pump and the heat transfer rates are higher in facilities where Therminol VP-1 is used. However, the property which affects the most to operational parameters of the HTF pump and

to heat transfer performance is the viscosity. With higher values of viscosity, more pumping power is required by the HTF since the centrifugal pump performance is reduced. Furthermore, higher values of viscosity imply a lower HTF convective heat transfer coefficient and therefore lower heat transfer rates. As a consequence, for the same operational conditions CSP plants using Syltherm 800 will obtain lower heat transfer rates, and will require more power for pumping the HTF, especially at the start-up of the CSP plant and at overnight, two critical periods where the HTF temperature has a significant decrease. The HTF specific heat and thermal conductivity do not affect to the operational parameters of the HTF pump. However, both parameters affect directly proportional to the thermal power transferred or absorbed by HTF. Syltherm 800 has lower values of specific heat and thermal conductivity than Therminol VP-1 which negatively affect the heat absorption and heat losses during the charging and discharging processes of the CPS plant. Finally, vapour pressure is the last key property to take into account for a proper operation of CSP plants. Vapour pressure affects directly proportional to the working pressure of the CSP plant. Low working pressures allow using thin tube walls, which reduces the wall temperature gradient and therefore the induced mechanical stress. Moreover, if the vapour pressure is too high, gas bubbling may appear in low pressure areas, such as the inlet of HTF pumps, and may increase the problems of cavitation. Syltherm 800 has higher values of vapour pressure than Therminol VP-1, which means that the operation pressure of CSP plant needs to be higher to prevent the above-mentioned problems.

As a conclusion, it can be stated that from the theoretical analysis of the thermophysical properties of both HTF, CSP plants using Therminol VP-1 will have a better performance than the ones using Syltherm 800 in terms of heat transfer rates and power consumption.

Table 6. Properties of Therminol VP-1 and Syltherm 800 based on the data given by the manufacturers

Properties	**Therminol VP-1**	**Syltherm 800**
Composition	Biphenyl and Diphenyl oxide	Dimethyl polysiloxane
Appearance	Clear, sediment free liquid	Clear yellow as supplied and darkened after extended use
Thermal stability	400 ºC	400ºC
Boiling point	257 ºC	203 ºC
Flash point	110 - 124 ºC	35 - 160 ºC
Fire point	127 ºC	193 ºC
Autoignition point	621 ºC	385 ºC
Crystallization point	12 ºC	-40 ºC
Density	$\rho(kg/m^3) = -2.835 \cdot 10^{-6} \cdot T^3(^oC) + 1.235 \cdot 10^{-3} \cdot T^2(^oC) + 1.037 \cdot T(^oC) + 1094$	$\rho(kg/m^3) = -1.671 \cdot 10^{-6} \cdot T^3(^oC) + 4.216 \cdot 10^{-4} \cdot T^2(^oC) - 0.917 \cdot T(^oC) + 953.17$
Kinematic viscosity	$v(m^2/s) = -9.565 \cdot 10^{-19} \cdot T^5(^oC) + 1.417 \cdot 10^{-15} \cdot T^4(^oC) - 8.435 \cdot 10^{-13} \cdot T^3(^oC) + 2.574 \cdot 10^{-10} \cdot T^2(^oC) - 4.197 \cdot 10^{-8} \cdot T(^oC) + 3.318 \cdot 10^{-6}$	$v(m^2/s) = -2.106 \cdot 10^{-18} \cdot T^5(^oC) + 3.322 \cdot 10^{-15} \cdot T^4(^oC) - 2.125 \cdot 10^{-12} \cdot T^3(^oC) + 7.061 \cdot 10^{-10} \cdot T^2(^oC) - 1.274 \cdot 10^{-7} \cdot T(^oC) + 1.095 \cdot 10^{-5}$
Specific heat	$cp(kJ/kg \cdot K) = 4.908 \cdot 10^{-11} \cdot T^4(^oC) - 3.960 \cdot 10^{-8} \cdot T^3(^oC) + 1.107 \cdot 10^{-5} \cdot T^2(^oC) + 1.439 \cdot 10^{-3} \cdot T(^oC) + 1.556$	$cp(kJ/kg \cdot K) = 1.706 \cdot 10^{-3} \cdot T(^oC) + 1.574$
Thermal conductivity	$\lambda(W/m \cdot K) = -1.687 \cdot 10^{-7} \cdot T^2(^oC) - 8.885 \cdot 10^{-5} \cdot T(^oC) + 0.138$	$\lambda(W/m \cdot K) = -1.881 \cdot 10^{-4} \cdot T(^oC) + 0.139$
Vapour pressure	$P_v(kPa) = 7.394 \cdot 10^{-5} \cdot T^3(^oC) - 3.527 \cdot 10^{-2} \cdot T^2(^oC) + 5.744 \cdot T(^oC) + 3.064 \cdot 10^2$	$P_v(kPa) = 2.754 \cdot 10^{-5} \cdot T^3(^oC) - 7.020 \cdot 10^{-4} \cdot T^2(^oC) + 0.866 \cdot T(^oC) + 75.37$

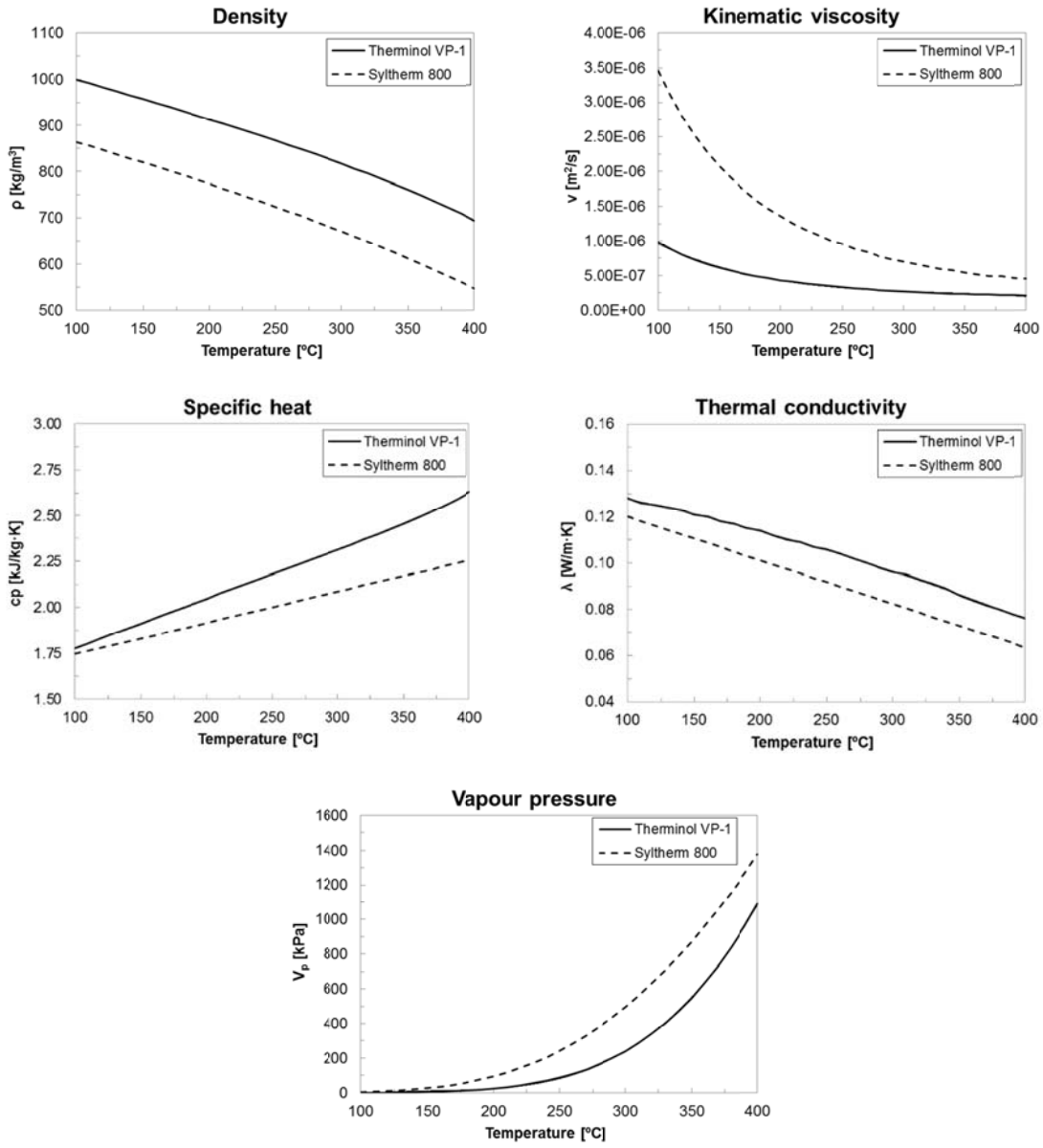

406 Figure 6. Main thermophysical properties comparison between Therminol VP-1 and Syltherm 800.

407

408 **5.2. Experimental results**

409 **5.2.1. HTF Pumping head**

410

417 Figure 7 shows the total head provided by the HTF pump during the charging process using
418 Therminol VP-1 and Syltherm 800. This parameter is equivalent to the difference of pressure
419 between the inlet and the outlet of the HTF pump. As it can be seen, for the same operational
420 conditions, the average head provided by the pump when Syltherm 800 was used, is 16,9 %
421 higher than the head provided when using Therminol VP-1, and therefore a higher pumping
422 power is required when Syltherm 800 is used. This result validates the statements presented in
423 the previous section. The oscillations observed in the values of the pump head shown in Figure

7 were due to the flow regulation though automatic three way valve, which is connected to a PID controller.

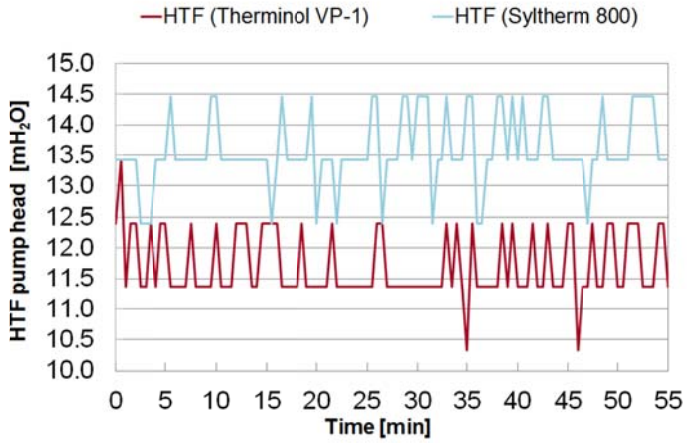

Figure 7. Total HTF pump head during the charging process for both fluid tested, Therminol VP-1 and Syltherm 800

5.2.2. Temperature profile

Figure 8 shows the temperature evolution of the molten salts and Therminol VP-1 studied at the PHEX during a charging process with a counter flow arrangement. Figure 9 shows a similar profile but with Syltherm 800. During the periods before and after the charging process, which are shaded in both figures, there was only HTF circulation through the PHEX. Therefore, the observed temperature values on the molten salts side were due to the influence of the electric tracing system and the HTF circulation on the temperature sensors. The charging process with both HTF lasted 40 min. Notice that when the steady-state period was reached, important differences were observed in the temperature profiles of both HTF. When Therminol VP-1 was used, the temperature difference at the hot tank side (represented by the temperature sensors HTF in and Salts out) was 5 ºC, while at the cold tank side (represented by temperature sensors HTF out and Salts in), the temperature difference was used was 4 ºC. However, when Syltherm 800 was used the temperature difference at the hot tank side was 14 ºC, while practically no difference was observed in the cold tank side. As explained in Ssection 5.1, Therminol VP-1 has higher thermal conductivity and lower viscosities than Syltherm 800. Therefore, there is a higher heat transfer rate between the molten salts and the Therminol, which makes the temperature gradient at the hot tank side to be lower.

Finally, the temperature profiles of the molten salts of both figures show characteristic peak at the beginning of the charging process (between 10 and 15 minutes), which is mainly due to the molten salts pump. At the early stages the pump does not provide instantly the desired flow rate,

but lower and, as a consequence, more energy is exchanged between the HTF and the molten salts. Afterwards, when the process is stabilized and the pump supplies the desired flow rate, the temperature decreases until it reaches stationary state.

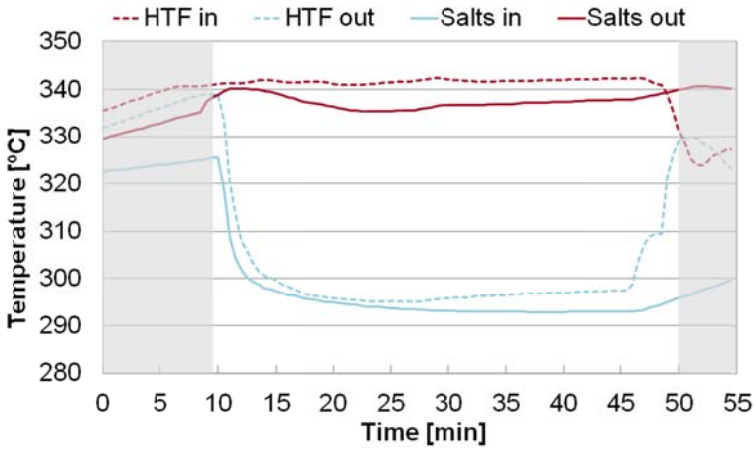

Figure 8. Temperature evolution of Therminol VP-1 and molten salts at the PHEX during the charging process with a counter flow arrangement. Shaded areas reflect the periods before and after the charging process.

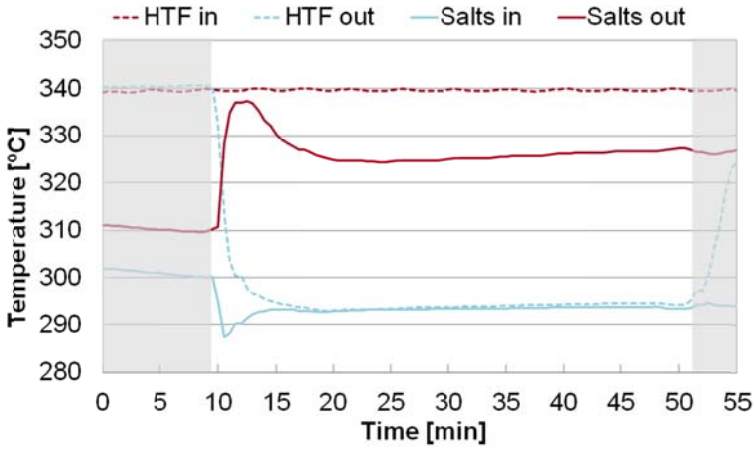

Figure 9. Temperature evolution of Syltherm 800 and molten salts at the PHEX during the charging process with a counter flow arrangement. Shaded areas reflect the periods before and after the charging process.

5.2.3. Power, energy, efficiency, and effectiveness

Figure 10 shows the evolution of the heat transfer rates and energy exchanged of both HTF and the molten salts during the charging process with a counter flow arrangement. At the fixed values of temperatures and HTF flow rates, the charging process using Therminol VP-1 as HTF showed higher values of heat transfer in both the HTF and molten salts fluids. Focusing on the specific values, Table 7 shows the summary of the heat transfer rates during this process. Notice that the average value of the power released by Therminol VP-1 was 9.37 kW, while the power released by Syltherm 800 was 6.82 kW, which gives a difference of 37.4% in the power

478 released by the HTF. However, the molten salts power absorbed by the molten salts when using
479 Therminol VP-1 as HTF was 8.11 kW, while the molten salts power absorbed by the molten
480 salts when using Syltherm 800 as HTF was 5.43 kW, which gives a difference of 49.4%. These
481 results validate the statements done in Section 5.1. However, there is a difference in the
482 percentage of increase depending on fluid, molten salt or HTF, studied. This difference is due to
483 a combination of the heat losses to the environment and the non-ideal performance of the
484 PHEX, which also causes the thermal efficiency ratio to be lower than 100 %. These values
485 were 79.6 % when using Syltherm 800 and 86.5 % when using Therminol VP-1. Regarding the
486 energy exchanged, the profiles have a linear tendency, as a result of the linear dependence to the
487 heat transfer rates. Therefore, the same statements than the ones done for the heat transfer rates
488 discussion can be done. Finally, the average effectiveness ratio when using Therminol VP-1 was
489 0.95 while the average effectiveness ratio when using Syltherm 800 was 0.87. This 9.19 %
490 difference follows the statements presented before.
479

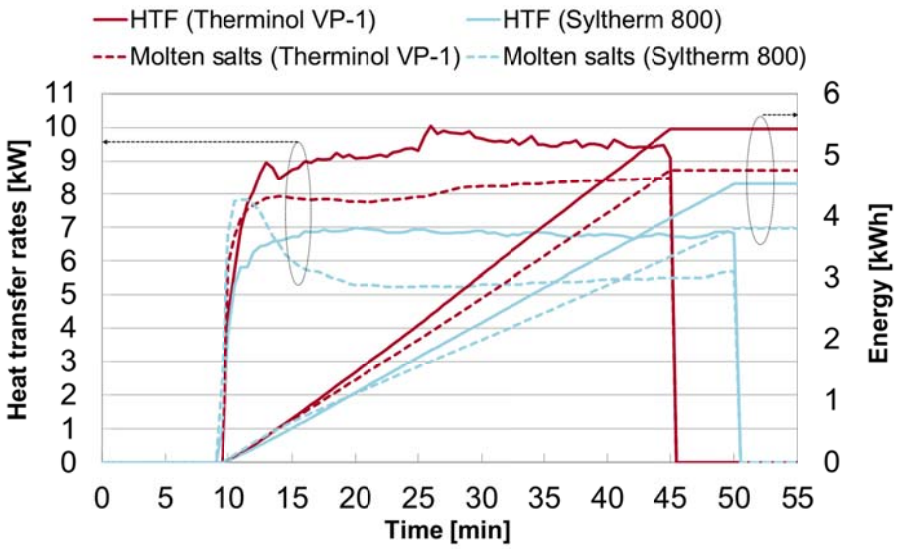

480

482 Figure 10. Heat transfer rate profiles of both HTF and molten salts during the charging process with a
483 counter flow arrangement
483

485 Table 7. Summary of the heat transfer rates and energy exchanged during the charging process with a
486 counter flow arrangement

	Therminol VP-1	**Syltherm 800**
Q_{HTF} [kW]	9.37	6.82
Q_{Salts} [kW]	8.11	5.43
E_{HTF} [kWh]	5.54	4.66
E_{Salts} [kWh]	4.80	3.71

5.2.4. Overall and convective heat transfer coefficients

Table 8 shows the overall heat transfer coefficients (U), obtained with the two methodologies explained in Section 4.2. In general, good agreement between the energy balance and correlation values for the overall heat transfer coefficient is observed in both processes, with a variation between the two methodologies of less than 3 %. This variation in the two proposed methodologies is within the range of uncertainty limit showed in Table 5 and therefore validates the experimental data obtained in the experimentation. Results from Table 8 show that the U-value during the charging process which used Therminol VP-1 as HTF is 48 % higher than the U-value during the charging process which used Syltherm 800. Similarly, the convective heat transfer coefficient at the HTF side of the PHEX during the charging process which used Therminol VP-1 as HTF is 74 % higher than the convective heat transfer coefficient at the HTF side of the PHEX during the charging process which used Syltherm 800 as HTF. However, the convective heat transfer coefficient at the molten salts side of the PHEX during the charging process which used Therminol VP-1 as HTF is 9.5 % higher than the convective heat transfer coefficient at the molten salts side of the PHEX during the charging process which used Syltherm as HTF due to small differences in the flow rate of the molten salts. These results showed the influence of the HTF thermophysical properties on the heat transfer rates in terms of its U-value and heat transfer coefficient. Finally, Table 8 also presents de Reynolds number of both HTF during the evaluated processes. These values show that both charging processes were carried out under turbulent regime, since they are higher than transition to turbulence limit for PHEX fixed at 400 by Kakaç et al. [24].

Table 8. Summary of the U-values (two methodologies), ~~and~~ convective heat transfer coefficients (correlatiosn only) and Reynolds number during the charging process with a counter flow arrangement

	Therminol VP-1	**Syltherm 800**
$\mathbf{U_{Exp}}$ **[W/m^2·ºC]**	583.53	390.22
$\mathbf{U_{Cor}}$ **[W/m^2·ºC]**	588.80	401.89
$\mathbf{h_{HTF}}$ **[W/m^2·ºC]**	1024.44	588.39
$\mathbf{h_{salts}}$ **[W/m^2·ºC]**	1432.86	1308.15
$\mathbf{Re_{HTF}}$ **[-]**	1963.81	827.52

6. Conclusions

In the present paper, the authors theoretically and experimentally compare two commercial HTF for industrial and CSP plants purposes: thermal oil Therminol VP-1 and silicone fluid Syltherm 800. The theoretical study consisted of an analytical comparison of the thermophysical properties of both HTF. The experimental study consisted of analysing the behaviour of both HTF in a two-tank molten salt pilot plant facility at the University of Lleida (Spain) during a charging process with a counter flow arrangement. The objective was to validate the statements obtained in the theoretical study.

From the theoretical study, the authors conclude that Therminol VP-1 is the best candidate for industrial and CSP purposes up to 400 ºC. For working temperatures below this value, Therminol VP-1 has lower viscosity and vapour pressure than Syltherm 800. Hence, the benefits turn to be lower electrical consumptions associated to the HTF pump, lower heat losses, and higher heat transfer rates. However, Therminol VP-1 presents a big disadvantage, which is that it presents its crystallization point at 12 ºC, which means that the OPEX of a CSP plant that uses this HTF will be higher because of the use of tracing systems in case of lower temperatures and presents higher toxicity for the user and for the environment.

During the experimental study, the authors compared during a charging process the following parameters: temperatures profiles, heat transfer, overall heat transfer coefficients, convective heat transfer coefficients, effectiveness, and efficiencies. The experimental results showed that the process which used Therminol VP-1 as HTF had a better behaviour, validating the theoretical study. Results showed a difference of 37.4 % in the heat transfer rate and 48 % in the overall heat transfer coefficients.

Acknowledgements

The research leading to these results has received funding from Spanish goverment (Fondo tecnológico IDI-20090393, ConSOLida CENIT 2008-1005) and from Abengoa Solar NT. The work is partially funded by the Spanish government (ENE2008-06687-C02-01/CON, ENE2011-22722, ULLE10-4E-1305 and ENE2015-64117-C5-1-R (MINECO/FEDER)). The authors would like to thank the Catalan Government for the quality accreditation given to their research group GREA (2014 SGR 123). This project has also received funding from the European Commission Seventh Framework Programme (FP/2007-2013) under Grant agreement NºPIRSES-GA-2013-610692 (INNOSTORAGE) and from the European Union's Horizon 2020

research and innovation programme under grant agreement No 657466 (INPATH-TES). Laia Miró would like to thank the Spanish Government for her research fellowship (BES-2012-051861). Jaume Gasia would like to thank the Departament d'Universitats, Recerca i Societat de la Informació de la Generalitat de Catalunya for his research fellowship (2017FI_B1 00092). The authors would like to thank Dr. Eduard Oró from Catalonia Institute for Energy Research (Spain) and Dr. Antoni Gil from Massachusetts Institute of Technology (USA) for their help during the initial stages of the experimentation.

References

1. A. Gil, M. Medrano, I. Martorell, A. Lázaro, P. Dolado, B. Zalba, L.F. Cabeza, State of the art on high temperature thermal energy storage for power generation. Part 1-Concepts, materials and modellization, Renew. Sustain. Energy Rev. 14 (2010) 31–55.
2. M. Medrano, A. Gil, I. Martorell, X. Potau, L.F. Cabeza, State of the art on high-temperature thermal energy storage for power generation. Part 2-Case studies, Renew. Sustain. Energy Rev. 14 (2010) 56-72.
3. M. Liu, N.H.S. Tay, S. Bell, M. Belusko, R. Jacob, G. Will, W. Saman, F. Bruno, Review on concentrating solar power plants and new developments in high temperature thermal energy storage technologies, Renew Sustain. Energy Rev. 53 (2016) 1411-1432.
4. G. Glatzmayer, Summary report for concentrating solar power thermal storage workshop-New Concepts and Materials for Thermal Energy Storage and Heat-Transfer Fluids, National Renewable Energy laboratory 2011 [NREL/TP- 5500-52134].
5. C. Prieto, R. Osuna, A.I. Fernández, L.F. Cabeza, Molten salt facilities, lessons learnt at pilot plant scale to guarantee commercial plants; Heat losses evaluation and correction, Renew. Energ. 94 (2016) 175-185.
6. L.F. Cabeza, C. Prieto, L. Miró, J. Gasia, G. Peiró, Design and start-up of two pilot plants for Molten Salts Storage Testing, ASME 10th International Conference on Energy Sustainability, collocated with the ASME Power Conference and the ASME 14th International Conference on Fuel Cell Science, Engineering and Technology. Volume 1 (2016) Article number 59268.
7. M. M. Rodríguez-García, M. Herrador-Moreno, E. Zarza-Moya, Lessons learnt during the design, construction and start-up phase of a molten salt testing facility, App. Therm. Eng. 62 (2014) 520–528.
8. U. Herrmann, B. Kelly, H. Price, Two-tank molten salt storage for parabolic trough solar power plants, Energy 29 (2004) 883-893.

9. C. Prieto, L. Miró, G. Peiró, E. Oró, A. Gil, L.F. Cabeza, Temperature distribution in molten salts tank for CSP plant, Sol Energy 135 (2016) 518-526.
10. H. Benoit, D. Spreafico, D. Gauthier,G. Flamant, Review of heat transfer fluid in tube – recievers used in concentrating solar thermal systems: Properties and heat transfer coefficients, Renew Sustain. Energy Rev. 55 (2016) 298–315.
11. K. Vignarooban, X. Xinhai, A. Arvay, K. Hsu, A.M. Kannan, Heat transfer fluids for concentrating solar power systems. A review, Appl. Energy 146 (2015) 383–396.
12. J. Gasia, L.,Miró, L.F. Cabeza, Review on system and materials requirements for high temperature thermal energy storage. Part 1: General requirements, Renew Sustain. Energy Rev. Accepted 2017.
13. S. Sau, N. Corsaro, T. Crescenzi, C. D'Ottavi, R. Liberatore, S. Licoccia,V. Russo, P. Tarquini, A.C.Tizzoni, Techno-economic comparison between CSP plants presenting two different heat transfer fluids, Appl Energy 168 (2016) 96–109.
14. G. Peiró, J. Gasia, L. Miró, C. Prieto, L.F. Cabeza, Experimental analysis of charging and discharging processes, with parallel and counter flow arrangements, in a molten salts high temperature pilot plant scale setup, Appl. Energy 178 (2016) 394-403.
15. Therminol. Therminol VP-1 Heat Transfer Fluid Product Information, https://www.therminol.com/products/Therminol-VP1; [accessed 02.12.16].
16. Syltherm 800. Heat Transfer Fluid product information. http://www.dow.com/heattrans/products/synthetic/syltherm.htm; [accessed 02.12.16].
17. Sigma-Aldrich. Diphenyl oxide information. http://www.sigmaaldrich.com/catalog/product/aldrich/w366706?lang=es&region=ES; [last accessed 15.03.16].
18. Sigma-Aldrich. Biphenyl information. http://www.sigmaaldrich.com/catalog/product/aldrich/w312908?lang=es&region=ES; [last accessed 15.03.16].
19. D. Kearney, U. Herrmann, P. Nava, B. Kelly, R. Mahoney, J. Pacheco, R. Cable, N. Potrovitza, D. Blake, H. Price, Assessment of a molten salt heat transfer fluid in a parabolic trough solar field, J. Sol Energy Eng. Trans. ASME 125 (2003) 170-176.
20. A.I. Fernandez, M. Martinez, M. Segarra, I. Martorell, L.F. Cabeza, Selection of materials with potential in sensible thermal energy storage, Sol Energ. Mat. Solar C. 94 (2010) 1723-1729.
21. R.W. Carting, C.M. Kramer, R.W. Bradshaw, D.A. Nissen, R.W. Goods, J.W. Munford R.N. Karnowsky, R.N. Biefeld, N.J. Norem, Molten nitrate salt technology development status report. Sandia National Laboratories Albuquerque (NM). 1981; Report No. SAND 80-8052.

620 22. B.D. Inverson, S.T. Broome, A.M. Kruizenga, J. G. Cordaro, Thermal and mechanical
621 properties of nitrate thermal storage salts in the solid-phase, Sol Energy 86 (2012) 2897-
622 2911.
623 23. Plate Heat exchanger. ALFANOVA HP 76-38H information product.
624 http://www.alfalaval.com/globalassets/documents/products/heat-transfer/plate-heat-
625 exchangers/fusion-bonded-plate-heat-
626 exchangers/alfanova76_productleaflet_che00048en.pdf; [last accessed 15.03.16]
627 24. S. Kakaç, H. Liu, Heat exchangers: selection, rating, and thermal design, first ed., CRC
628 Press LLC, Florida (USA), 1998, pp. 323-351.
629 25. A.K. Tiwari, G. Pradvumna, J. Sarkar, Performance comparison of the plate heat exchanger
630 using different nanofluids, Exp. Therm. Fluid Sci. 49 (2013)141-151.
631 26. A.K. Tiwari, G. Pradvumna, J. Sarkar, Heat transfer and pressure drop characteristics of
632 CeO_2/water nanofluid in plate heat exchanger, App. Therm. Eng. 57 (2013) 24-32.
633 27. R. Serrano-López, J. Fradera, S. Cuesta-López, Molten salts data for energy applications,
634 Chem. Eng. Process. 73 (2013) 87–102.
635 28. J.P. Holman, Experimental Methods for Engineers, eight ed. McGrawHill, Newyork, 2012.
636